Nuclear Science and Techniques (2024) 35:99
https://doi.org/10.1007/s41365-024-01455-9

A possible probe to neutron-skin thickness by fragment parallel momentum distribution in projectile fragmentation reactions

Chun-Wang Ma[1,2] · Yi-Jie Duan[1] · Ya-Fei Guo[1] · Chun-Yuan Qiao[1] · Yu-Ting Wang[1] · Jie Pu[1] · Kai-Xuan Cheng[1] · Hui-Ling Wei[1]

Received: 6 December 2023 / Revised: 4 March 2024 / Accepted: 7 March 2024 / Published online: 18 June 2024

Abstract
Neutron-skin thickness is a key parameter for a neutron-rich nucleus; however, it is difficult to determine. In the framework of the Lanzhou Quantum Molecular Dynamics (LQMD) model, a possible probe for the neutron-skin thickness (δ_{np}) of neutron-rich ^{48}Ca was studied in the 140*A* MeV ^{48}Ca + ^{9}Be projectile fragmentation reaction based on the parallel momentum distribution ($p_{\|}$) of the residual fragments. A Fermi-type density distribution was employed to initiate the neutron density distributions in the LQMD simulations. A combined Gaussian function with different width parameters for the left side (Γ_{L}) and the right side (Γ_{R}) in the distribution was used to describe the $p_{\|}$ of the residual fragments. Taking neutron-rich sulfur isotopes as examples, Γ_{L} shows a sensitive correlation with δ_{np} of ^{48}Ca, and is proposed as a probe for determining the neutron skin thickness of the projectile nucleus.

Keywords Neutron-skin thickness · Projectile fragmentation · Parallel momentum distribution · Neutron-rich nucleus · Quantum molecular dynamics model

1 Introduction

The neutron skin thickness, defined as the difference between the root mean square of the neutron and proton density distributions of a nucleus $\delta_{\mathrm{np}} \equiv \langle r_{\mathrm{n}}^2\rangle^{1/2} - \langle r_{\mathrm{p}}^2\rangle^{1/2}$, is an important parameter for neutron-rich nuclei. With the advanced ability of new rare isotope facilities to produce nuclei near proton and neutron drip lines, a new era has commenced for nuclei with exotic structures, particularly for neutron-rich isotopes at extremes [1, 2]. The exact value of δ_{np} is important in research on symmetry energy [3] and neutron stars [4]. It is more important to study δ_{np} of extreme nuclei because they may have a much lower density distribution in the surface region than stable nuclei. Along the history of studying δ_{np} of neutron-rich nuclei, many probes have been proposed based on different theoretical frameworks and via different types of experiments. Projectile fragmentation reactions induced by neutron-proton asymmetric nuclei, as one type of heavy-ion reactions, are typical experimental tools to investigate properties of neutron-rich nuclei, in which the light particle emissions [5, 6], fragment production ratios [7, 8], fragment mass or charge distributions through information entropy analysis [9, 10], etc, are proposed as probes to study the neutron-skin of projectile nuclei to varying degrees of accuracy. Due to the difficulties in measuring neutron density distributions, the neutron-skin thickness of asymmetric nuclei are usually determined in experiments through indirect probes, for example, the giant dipole resonance [11, 12], spin dipole resonance [13], neutron-removal cross section [14], and parity violating electron scattering (for ^{208}Pb [15, 16] and for ^{48}Ca [17]), etc. The momentum distribution of nucleons is widely used to study the structure and properties of atomic nuclei

This work was supported by the National Natural Science Foundation of China (Nos. 12375123, 11975091, and 12305130), the Natural Science Foundation of Henan Province (No. 242300421048), China Postdoctoral Science Foundation (No. 2023M731016), and Henan Postdoctoral Foundation (No. HN2022164).

✉ Chun-Wang Ma
machunwang@126.com

1 College of Physics, Henan Normal University, Xinxiang 453007, China

2 Institute of Nuclear Science and Technology, Henan Academy of Sciences, Zhengzhou 450015, China

[18–21]. The short-range correlation between nucleons can be experimentally studied by detecting the high-momentum tail of the nucleon momentum distribution using bremsstrahlung γ rays in heavy-ion nuclear reactions [22–24]. The parallel momentum distribution ($p_{\parallel}$) of fragments in breakup or few-body reactions is usually the first evidence of halo or skin nuclei, as in ^{11}Li [18], ^{29}P [25], ^{23}Al [26], ^{31}Ne [27]. Thus, $p_{\parallel}$ of the residual fragments can also be employed to determine $\delta_{\rm np}$ within the framework of optical models [28–30]. Experimentally, the $p_{\parallel}$ of fragments is usually used to determine their yields or cross-sections after integration [31], which directly connects the yields of fragments and the nuclear density (and neutron skin thickness) of the projectile nucleus. This makes the $p_{\parallel}$ of fragment in potential be a probe for $\delta_{\rm np}$ of projectile nucleus. In this study, $p_{\parallel}$ of the residual fragments in projectile fragmentation reactions was investigated using the Lanzhou quantum molecular dynamics (LQMD) model [32, 33]. It is suggested that the width of $p_{\parallel}$ of the fragment produced in the peripheral collisions is sensitive and could serve as a probe for $\delta_{\rm np}$ of the projectile nucleus.

2 Model description

2.1 The LQMD model

The LQMD model is an isospin- and momentum-dependent transport model that includes all possible elastic and inelastic collision reaction channels during charge exchange. The temporal evolution of nucleons, hyperons, and mesons in a reaction system under a self-consistently generated mean field is governed by Hamilton's equations of motion [32–35]. Based on the Skyrme interactions, isospin-, density-, and momentum-dependent Hamiltonians were constructed [34]. The Hamiltonian of baryons consists of the relativistic energy, effective interaction potential, and momentum-related components.

$$H_{\rm B} = \sum_i \sqrt{\mathbf{p}_i^2 + m_i^2} + U_{\rm int} + U_{\rm mom}, \tag{1}$$

where $\mathbf{p}_i$ and m_i denote the momentum and mass of the baryons, respectively. $U_{\rm int}$ comprises the Coulomb interaction and the local interaction potential. The local interaction potential is expressed as follows:

$$U_{\rm loc} = \int V_{\rm loc}[\rho(\mathbf{r})]d\mathbf{r}, \tag{2}$$

derived from the Skyrme energy density functional. $V_{\rm loc}(\rho)$ can be written as:

$$\begin{aligned} V_{\rm loc}(\rho) =& \frac{\alpha}{2}\frac{\rho^2}{\rho_0} + \frac{\beta}{1+\gamma}\frac{\rho^{1+\gamma}}{\rho_0^{\gamma}} + E_{\rm sym}^{\rm loc}(\rho)\rho\delta^2 \\ &+ \frac{g_{\rm sur}}{2\rho_0}(\nabla\rho)^2 + \frac{g_{\rm sur}^{\rm iso}}{2\rho_0}[\nabla(\rho_{\rm n} - \rho_{\rm p})]^2, \end{aligned} \tag{3}$$

where $\rho_{\rm n}$, $\rho_{\rm p}$ and $\rho = \rho_{\rm n} + \rho_{\rm p}$ are the neutron, proton, and total densities, respectively, and $\delta = (\rho_{\rm n} - \rho_{\rm p})/(\rho_{\rm n} + \rho_{\rm p})$ is isospin asymmetry. The coefficients $\alpha, \beta, \gamma, g_{\rm sur}, g_{\rm sur}^{\rm iso}$, and ρ_0 were set to −215.7 MeV, 142.4 MeV, 1.32223 MeV fm^2, −2.7 MeV fm^2, and 0.16fm^{-3}, respectively. $E_{\rm sym}^{\rm loc}(\rho)$ is the local part of the symmetry energy, which can be adjusted to mimic the predictions of the symmetry energy calculated using microscopic or phenomenological many-body theories.

$$E_{\rm sym}^{\rm loc}(\rho) = \frac{1}{2}C_{\rm sym}(\rho/\rho_0)^{\gamma_{\rm s}}. \tag{4}$$

The values of $C_{\rm sym}$ and $\gamma_{\rm s}$ are 52.5 MeV and 2.0, respectively, which correspond to hard-symmetry energy with a baryon density [34].

$U_{\rm mom}$ takes the form

$$\begin{aligned} U_{\rm mom} =& \frac{1}{2\rho_0}\sum_{i,j,j\neq i}\sum_{\tau,\tau'} C_{\tau,\tau'}\delta_{\tau,\tau_i}\delta_{\tau',\tau_j}\int\int\int {\rm d}\mathbf{p}{\rm d}\mathbf{p}'{\rm d}\mathbf{r} \\ &\times f_i(\mathbf{r},\mathbf{p},t)\ln[\epsilon(\mathbf{p}-\mathbf{p}')^2 + 1]^2 f_i(\mathbf{r},\mathbf{p}',t), \end{aligned} \tag{5}$$

where $C_{\tau,\tau} = C_{\rm mom}(1+x)$, $C_{\tau,\tau'} = C_{\rm mom}(1-x)(\tau \neq \tau')$ and the isospin symbols $\tau(\tau')$ represent protons and neutrons, respectively. The parameters $C_{\rm mom}$ and ϵ were determined by fitting the real part of the optical potential as a function of the incident energy from the proton-nucleus elastic scattering data, and the obtained values of $C_{\rm mom}$ and ϵ were 1.76 MeV and 500 c^2/GeV^2, respectively. Thus, the effective mass of the nuclear medium at saturation density is m^*/m =0.75. The parameter x is the strength of the isospin splitting, for which a value of −0.65 is adopted in this study, and the mass splitting is $m_{\rm n}^* > m_{\rm p}^*$ in the nuclear medium [36].

During the initialization of the projectile nucleus in LQMD, the initial coordinates of the nucleons are obtained by random sampling according to the two-parameter Fermi-type density distribution [38]:

$$\rho_i(r) = \frac{\rho_i^0}{1 + \exp\left(\frac{r - C_i}{f_i t_i/4.4}\right)}, i = {\rm n}, {\rm p}, \tag{6}$$

where ρ_i^0 is a normalization constant that ensures that the integrated density distribution is equal to the number of protons or neutrons, f_i is a parameter for adjusting the diffuseness parameter [7, 39], t_i is the diffuseness parameter, C_i is the half-density radius. Nuclei with reliable stability and an

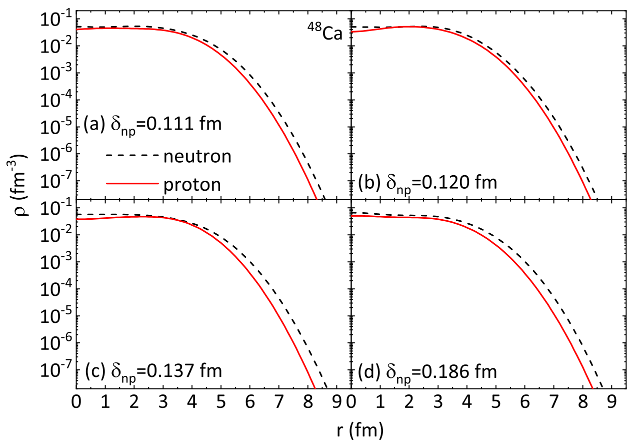

Fig. 1 (Color online) The proton and neutron physical density distributions in the initialization of ^{48}Ca in the LQMD simulation with different δ_{np}. In **a–d**, δ_{np} are 0.111, 0.120, 0.137, and 0.186 fm, respectively

expected neutron skin thickness were selected as candidates for collisions, and the values of δ_{np} were 0.111, 0.120, 0.136, 0.168, and 0.186 fm for the corresponding initial ^{48}Ca nuclei after LQMD initialization (see Fig. 1). The fragments were analyzed in phase space at $t = 300$ fm/c in the LQMD simulation, and nucleons with a relative distance smaller than 3.0 fm and a relative momentum smaller than 200 MeV/c were considered in the coalescence model [33].

2.2 Parallel momentum distribution

The $p_{\parallel}$ of the fragments produced in projectile fragmentation reactions exhibits a nonsymmetric distribution in experiments, which can be fitted by a combined Gaussian function [31],

$$\frac{d\Gamma}{dp} = \begin{cases} S \times \exp\left(-\frac{(p-p_0)^2}{2\Gamma_L^2}\right), & \text{if } p \le p_0, \\ S \times \exp\left(-\frac{(p-p_0)^2}{2\Gamma_R^2}\right), & \text{if } p > p_0. \end{cases} \tag{7}$$

In the combined Gaussian function, the left and right halves have the same peak position, but different widths. S is the normalization factor, p_0 is the peak position of the distribution, Γ_L and Γ_R denote the widths of the left and right sides of the combined Gaussian distribution, respectively.

3 Results and discussion

$p_{\parallel}$ of a fragment is generally influenced by the incident energy of the reaction, nuclear density of the reaction system, impact parameter, and the fragment itself (such as isospin). The experimental δ_{np} determined from the proton elastic scattering for ^{40}Ca was $-0.010^{+0.022}_{-0.024}$ fm [37], and for ^{48}Ca, it was 0.121 ± 0.026(exp) $\pm$ 0.024(model) fm from the parity-violating method [17]. To compare the sensitivity of $p_{\parallel}$ to the projectile nuclear density distribution, the ^{33}P produced in the 140A MeV ^{40}Ca + ^{9}Be ($\delta_{np} = -0.030$ fm of ^{40}Ca) and ^{48}Ca + ^{9}Be ($\delta_{np} = 0.168$ fm of ^{48}Ca) reactions are simulated and fitted by Eq. (7), as shown in Fig. 2. $p_{\parallel}$ for ^{33}P in the symmetric ^{40} Ca-induced reaction is also symmetric in Γ_L and Γ_R, whereas Γ_L is larger than Γ_R for ^{33}P in the asymmetric ^{48} Ca-induced reaction, indicating a neutron-skin effect for the neutron-rich projectile.

With the varying impact parameters in projectile fragmentation reactions, the $p_{\parallel}$ of a specific fragment is also influenced by the significant change in nuclear density from central to peripheral collisions [23], and the $p_{\parallel}$ of a fragment thus carries significant information on reactions, such as nuclear density distribution and nucleon-nucleon cross section [1]. The $p_{\parallel}$ values of the neutron-proton symmetric fragment ^{24}Mg produced in the 140A MeV ^{48}Ca + ^{9}Be reaction within $b = [0–2]$, [2–4], [4–6], and [6–8] fm are plotted in Fig. 3. From the central to the peripheral collisions, $p_{\parallel}$ for ^{24}Mg shifts from the low-momentum side to the high-momentum side as b increases. Both Γ_L and Γ_R depend on impact parameters. For different $p_{\parallel}$, the value of Γ_L tends to decrease with an increase in b. $\Gamma_L > \Gamma_R$ (Fig. 3), with the uncertainty of the Γ_R larger than that of Γ_L, (particularly for the central collisions). Γ_R remains constant when $b < 6$

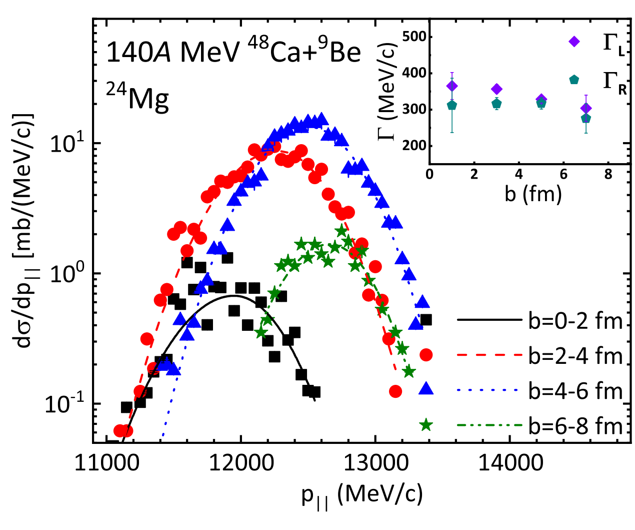

Fig. 2 (Color online) The $p_{\parallel}$ of ^{33}P fragments produced in the LQMD model simulated 140A MeV ^{40,48}Ca + ^{9}Be reactions within $b = [1–8]$ fm. The circles and triangles denote results for the ^{33}P fragments in the ^{48}Ca ($\delta_{np} = 0.168$ fm) and ^{40}Ca ($\delta_{np} = -0.030$ fm) induced reactions, respectively. The lines with different types denote the fitting results by a function according to Eq. (7)

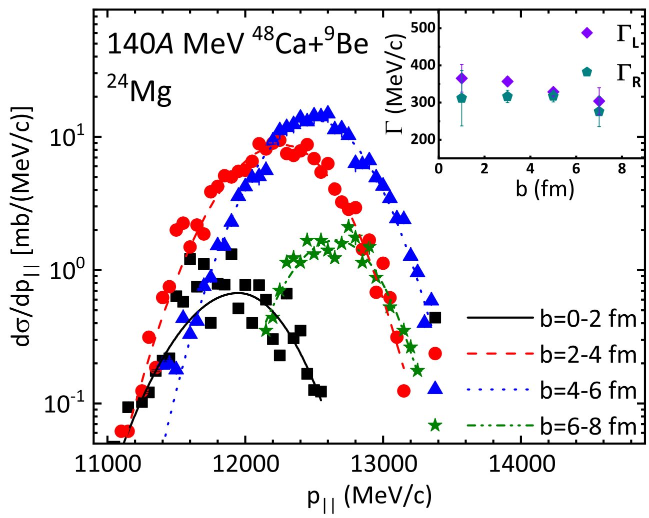

Fig. 3 (Color online) The $p_{\parallel}$ for ^{24}Mg produced in the 140A MeV ^{48}Ca + ^{9}Be (δ_{np} = 0.111 fm of ^{48}Ca) projectile fragmentation reactions at different ranges of impact parameter from central collisions to peripheral collisions. The ranges of b are within [0–2], [2–4], [4–6], and [6–8] fm, respectively. The lines of different types denote the fitting results by a function according to Eq. (7). The inserted figure are for Γ_L and Γ_R for the $p_{\parallel}$

fm whereas Γ_L decreases with increasing b. The reason for $\Gamma_L > \Gamma_R$ may be the difference in the centrality in the reaction; that is, the larger the centrality, the deeper the collision with the target, and the significant $p_{\parallel}$ lost, as well as the wider width of Γ_L.

Finally, the $p_{\parallel}$ values for the isotopic fragments with different isospins were studied to determine whether they are sensitive to the neutron skin thickness of the projectile. The neutron skin of the asymmetric nucleus mainly influences the products of peripheral collisions. The $p_{\parallel}$ of the fragments was simulated for peripheral collisions of 140A MeV ^{48}Ca + ^{9}Be within b = [6–8] fm. To compare $p_{\parallel}$ values for isotopic fragments with different mass numbers, $p_{\parallel}$ per nucleon ($p_{\parallel}/A$) was chosen. Based on the different values of δ_{np} for ^{48}Ca, as shown in Fig. 1, the $p_{\parallel}/A$ distributions for neutron-rich sulfur isotopes (from ^{33}S to ^{36}S) are plotted in Fig. 4 together with the fitting results by Eq. (7). The values of Γ_L for $p_{\parallel}$ were obtained and the Γ_L correlations for the sulfur isotopes with δ_{np} of ^{48}Ca are plotted in Fig. 5, in which the correlations are fitted using the decaying exponential function. A strong exponential dependence of Γ_L for neutron-rich sulfur isotopes on δ_{np} of the projectile nucleus ^{48}Ca is shown, which indicates that Γ_L can be an effective probe for the neutron skin thickness of the projectile nucleus in the projectile fragmentation reaction. Further simulations of the fragment de-excitation were performed using the GEMINI code [40]. Compared with the obvious correlation between Γ_L and δ_{np} in the LQMD simulations, Γ_L becomes constant as δ_{np} varies in the LQMD + GEMINI simulations, indicating that the GEMINI de-excitation erases the correlation between Γ_L and δ_{np}. It is also noted that the correlation between Γ_L and δ_{np} is an indirect probe for the neutron-skin thickness of the projectile nucleus because fragments are obtained after the compression-expansion process of the colliding system.

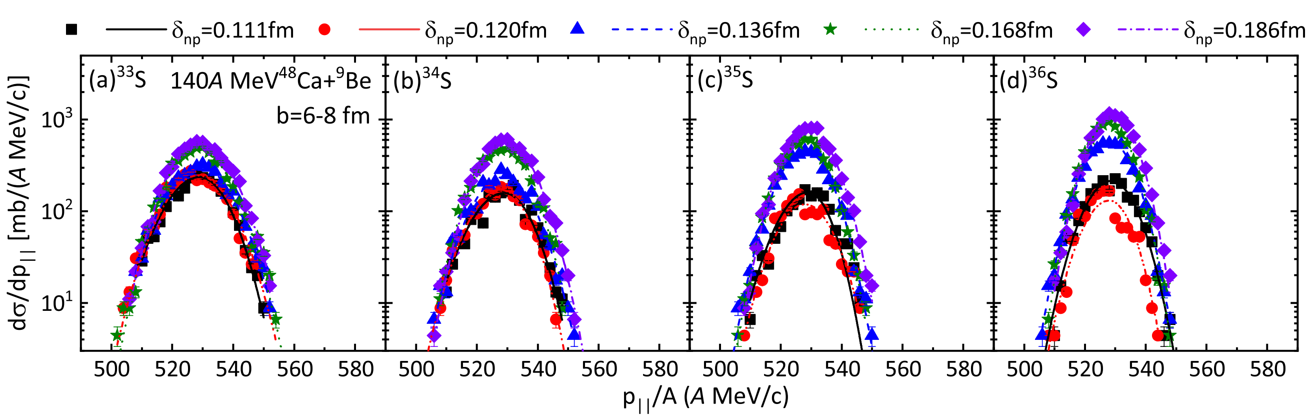

Fig. 4 (Color online) The LQMD simulated $p_{\parallel}/A$ in peripheral collisions (within b = [6–8] fm) for the 140A MeV ^{48}Ca + ^{9}Be reaction. The values of δ_{np} for ^{48}Ca are 0.111, 0.120, 0.136, 0.168, and 0.186 fm, respectively. **a** is for ^{33}S, **b** for ^{34}S, **c** for ^{35}S, and **d** for ^{36}S. The lines denote the fitting results by Eq. (7)

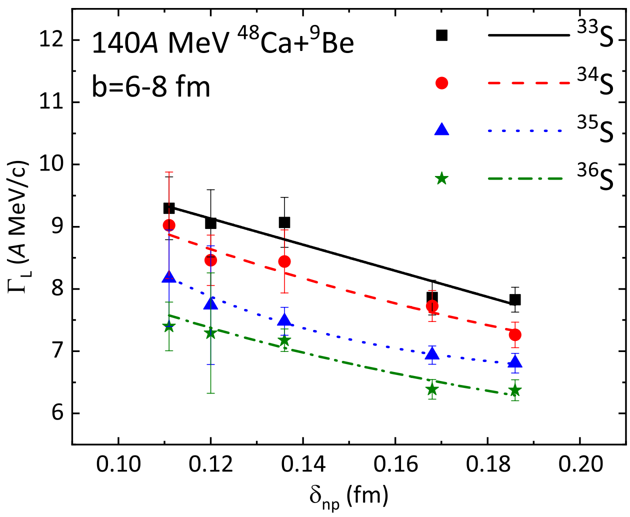

Fig. 5 (Color online) The correlation between Γ_L of $p_{\|}$ for neutron-rich sulfur fragments in Fig. 4 and δ_{np} of ^{48}Ca in the LQMD simulated peripheral collisions for 140*A* MeV ^{48}Ca + ^{9}Be reactions within $b = [6\text{–}8]$ fm. The lines of different types denote the exponential fits to the correlations for $^{33-36}$S

Further investigations are also needed to study the $\Gamma_L \sim \delta_{np}$ correlation, including the de-excitation effects, since they may modify the intermediate mass fragments in projectile fragmentation reactions, as has been found in Refs. [7, 8].

Based on the eikonal distorted-wave impulse approximation (DWIA) explanation by Ogata et al. [30], the high-momentum side reflects the phase-volume effect owing to energy and momentum conservation, whereas the low-momentum side reflects the momentum shift caused by the attractive potential of the residual nucleus when the incident energy is not very high (below 200*A* MeV). Because the impact parameters are restricted to $b = [6\text{–}8]$ fm, the width of Γ_L reflects the Heisenberg uncertainty principle in quantum mechanism; that is, from $\Delta x \cdot \Delta p \geq \frac{h}{4\pi}$, Δx is inversely correlated to Δp [21]. Thus, it can be considered that the larger the Γ_L, the closer the nucleons contained in the fragment are to the center of the nucleus. In contrast, the smaller the Γ_L, the closer the nucleons in the fragment to the edge of the nucleus. With an increased neutron-skin thickness, the valence neutrons are further pushed away from the center of the nucleus, resulting in a narrower Γ_L as observed in Fig. 4 for the neutron-rich sulfur fragments.

4 Summary

In summary, a possible probe for the neutron skin thickness of a neutron-rich projectile nucleus was studied by simulating the 140*A* MeV ^{48}Ca + ^{9}Be reaction in the framework of the LQMD model. The neutron skin thickness of ^{48}Ca was adjusted by varying the diffuseness of the neutron density distributions. A combined Gaussian function with different widths of the left (Γ_L) and right (Γ_R) halves was employed to fit $p_{\|}$ of the fragments. The $p_{\|}$ values of the fragments are influenced by the projectile nucleus, impact parameters, and the isospin of isotope. It was found that Γ_L of the $p_{\|}$ of the projectile-like fragments produced in peripheral collisions was sensitive to δ_{np} of the projectile nucleus. Considering that $p_{\|}$ of fragments is easy to measure in experiments, the correlation between Γ_L of the projectile-like fragments and δ_{np} of the projectile nucleus potentially provides a new probe for the neutron skin thickness of neutron-rich projectile nuclei.

Acknowledgements Ma and Duan thank Prof. Jun-Long Tian of Guangxi Normal University for useful discussions on the manuscript preparation and revisions.

Author Contributions All authors contributed to the study conception and design. Material preparation, data collection and analysis were performed by Chun-Wang Ma, Yi-Jie Duan, Ya-Fei Guo, Chun-Yuan Qiao, Yu-Ting Wang, Jie Pu, Kai-Xuan Chen and Hui-Ling Wei. The first draft of the manuscript was written by Chun-Wang Ma and all authors commented on previous versions of the manuscript. All authors read and approved the final manuscript.

Data Availability The data that support the findings of this study are openly available in Science Data Bank at https://cstr.cn/31253.11.sciencedb.j00186.00509 and https://doi.org/10.57760/sciencedb.j00186.00509.

Conflict of interest Chun-Wang Ma is an editorial board member for Nuclear Science and Techniques and was not involved in the editorial review, or the decision to publish this article. All authors declare that there are no Conflict of interest.

References

1. C.W. Ma, H.L. Wei, X.Q. Liu et al., Nuclear fragments in projectile fragmentation reactions. Prog. Part. Nucl. Phys. **121**, 103911 (2021). https://doi.org/10.1016/j.ppnp.2021.103911
2. X.B. Wei, H.L. Wei, Y.T. Wang et al., Multiple-models predictions for drip line nuclides in projectile fragmentation of ^{40,48}Ca, ^{58,64}Ni, and ^{78,86}Kr at 140 MeV/u. Nucl. Sci. Tech. **33**, 155 (2022). https://doi.org/10.1007/s41365-022-01137-4
3. L. Li, F.Y. Wang, Y.X. Zhang, Isospin effects on intermediate mass fragments at intermediate energy-heavy ion collisions. Nucl. Sci. Tech. **33**, 58 (2022). https://doi.org/10.1007/s41365-022-01050-w
4. W.J. Xie, Z.W. Ma, J.H. Guo, Bayesian inference of the crust-core transition density via the neutron-star radius and neutron-skin thickness data. Nucl. Sci. Tech. **34**, 91 (2023). https://doi.org/10.1007/s41365-023-01239-7
5. X.Y. Sun, D.Q. Fang, Y.G. Ma et al., Neutron/proton ratio of nucleon emissions as a probe of neutron skin. Phys. Lett. B **682**, 396 (2010). https://doi.org/10.1016/j.physletb.2009.11.031
6. D.Q. Fang, Neutron skin thickness and its effects in nuclear reactions. Nucl. Tech. **46**, 155 (2023) (in Chinese). https://doi.org/10.11889/j.0253-3219.2023.hjs.46.080016

7. Z.T. Dai, D.G. Fang, Y.G. Ma et al., Triton/^{3}He ratio as an observable for neutron-skin thickness. Phys. Rev. C **89**, 014613 (2014). https://doi.org/10.1103/PhysRevC.89.014613
8. Z.T. Dai, D.Q. Fang, Y.G. Ma et al., Effect of neutron skin thickness on projectile fragmentation. Phys. Rev. C **91**, 034618 (2015). https://doi.org/10.1103/PhysRevC.91.034618
9. C.W. Ma, Y.P. Liu, H.L. Wei et al., Determination of neutron-skin thickness using configurational information entropy. Nucl. Sci. Tech. **33**, 6 (2022). https://doi.org/10.1007/s41365-022-00997-0
10. H.L. Wei, X. Zhu, C. Yuan, Configurational information entropy analysis of fragment mass cross distributions to determine the neutron skin thickness of projectile nuclei. Nucl. Sci. Tech. **33**, 111 (2022). https://doi.org/10.1007/s41365-022-01096-w
11. A. Krasznahorkay, J. Bacelar, J.A. Bordewijk et al., Excitation of the isovector giant dipole resonance by inelastic α scattering and the neutron skin of nuclei. Phys. Rev. Lett. **66**, 1287 (1991). https://doi.org/10.1103/PhysRevLett.66.1287
12. M. Csatlós, A. Krasznahorkay, D. Sohler et al., Measurement of neutron-skin thickness in ^{208}Pb by excitation of the GDR via inelastic α-scattering. Nucl. Phys. A **719**, 304c (2003). https://doi.org/10.1016/S0375-9474(03)00937-0
13. C. Gaarde, J. Rapaport, T.N. Taddeucci et al., Excitation of giant spin-isospin multipole vibrations. Nucl. Phys. A **369**, 258 (1981). https://doi.org/10.1016/0375-9474(81)90019-1
14. D.Q. Fang, Y.G. Ma, X.Z. Cai et al., Effects of neutron skin thickness in peripheral nuclear reactions. Chin. Phys. Lett. **28**, 102102 (2011). https://doi.org/10.1088/0256-307X/28/10/102102
15. S. Abrahamyan, Z. Ahmed, H. Albataineh et al., Measurement of the neutron radius of ^{208}Pb through parity violation in electron scattering. Phys. Rev. Lett. **108**, 112502 (2012). https://doi.org/10.1103/PhysRevLett.108.112502
16. D. Adhikari, H. Albataineh, D. Androic et al., (PREX Collaboration), Accurate determination of the neutron skin thickness of ^{208}Pb through parity-violation in electron scattering. Phys. Rev. Lett. **126**, 172502 (2021). https://doi.org/10.1103/PhysRevLett.126.172502
17. D. Adhikari, H. Albataineh, D. Androic et al., (CREX Collaboration), Precision Determination of the Neutral Weak Form Factor of ^{48}Ca. Phys. Rev. Lett. **129**, 042501 (2022). https://doi.org/10.1103/PhysRevLett.129.042501
18. I. Tanihate, H. Hamagaki, O. Hashimoto et al., Measurements of interaction cross sections and nuclear radii in the light p-shell region. Phys. Rev. Lett. **55**, 2676 (1985). https://doi.org/10.1103/PhysRevLett.55.2676
19. E. Hanelt, A. Grewe, K.H. Schmidt et al., Momentum distributions of projectile fragments produced in the cold and hot fragmentation of relativistic ^{136}Xe and ^{197}Au projectiles. Z. Phys. A **346**, 43 (1993). https://doi.org/10.1007/BF01290780
20. Y.G. Ma, R. Wada, K. Hagel et al., Sequential decay distortion of Goldhaber model widths for spectator fragments. Phys. Rev. C **65**, 051602 (2002). https://doi.org/10.1103/PhysRevC.65.051602
21. M.Q. Ding, D.Q. Fang, Y.G. Ma, Effects of neutron-skin thickness on light-particle production. Phys. Rev. C **109**, 024616 (2024). https://doi.org/10.1103/PhysRevC.109.024616
22. O. Hen, G.A. Miller, E. Piasetzky et al., Nucleon-nucleon correlations, short-lived excitations, and the quarks within. Rev. Mod. Phys. **89**, 045002 (2017). https://doi.org/10.1103/RevModPhys.89.045002
23. Y.H. Qin, Q.L. Niu, D. Guo et al., Probing high-momentum component in nucleon momentum distribution by neutron-proton bremsstrahlung γ-rays in heavy ion reactions. Phys. Lett. B **850**, 138514 (2024). https://doi.org/10.1016/j.physletb.2024.138514
24. D.W. Si, Y. Zhou, S. Xiao et al., Measurement of the high energy γ -rays from heavy ion reactions using Čerenkov detector. Nucl. Sci. Tech. **35**, 24 (2024). https://doi.org/10.1007/s41365-024-01368-7
25. Y.B. Wei, Y.G. Ma, X.Z. Cai *et al*., Parallel momentum distribution of ^{28}Si Fragments from ^{29}P. Chin. Phys. Lett. **22**, 61 (2005). http://iopscience.iop.org/0256-307X/22/1/018
26. D.Q. Fang, W. Guo, C.W. Ma *et al*., Studies on the exotic structure of ^{23}Al. Chin. Phys. C **32**, 34 (2008). http://csnsdoc.ihep.ac.cn/article/id/68c4071e-1596-4366-8926-9446db4e3d07
27. S.Y. Zhang, S.S. Zhang, X.X. Sun et al., Study of the deformed halo nucleus ^{31}Ne with Glauber model based on microscopic self-consistent structures. Sci. China Phys. Mech. Astron. **65**, 262011 (2022). https://doi.org/10.1007/s11433-022-1894-6
28. B. Abu-Ibrahim, Y. Ogawa, Y. Suzuki et al., Cross section calculations in Glauber model: I. Core plus one-nucleon case. Comp. Phys. Commun. **151**, 369 (2003). https://doi.org/10.1016/S0010-4655(02)00734-8
29. K. Hencken, G. Bertsch, H. Esbensen, Breakup reactions of the halo nuclei ^{11}Be and ^{8}B. Phys. Rev. C **54**, 3043 (1996). https://doi.org/10.1103/PhysRevC.54.3043
30. K. Ogata, K. Yoshida, K. Minomo, Asymmetry of the parallel momentum distribution of (p, pN) reaction residues. Phys. Rev. C **92**, 034616 (2015). https://doi.org/10.1103/PhysRevC.92.034616
31. M. Mocko, M. Andronenko, F. Delaunay et al., Projectile fragmentation of ^{40}Ca, ^{48}Ca, ^{58}Ni, and ^{64}Ni at 140 MeV/nucleon. Phys. Rev. C **74**, 054612 (2006). https://doi.org/10.1103/PhysRevC.74.054612
32. Z.Q. Feng, Momentum dependence of the symmetry potential and its influence on nuclear reactions. Phys. Rev. C **84**, 024610 (2011). https://doi.org/10.1103/PhysRevC.84.024610
33. Z.Q. Feng, Effects of isospin dynamics on neck fragmentation in isotopic nuclear reactions. Phys. Rev. C **94**, 014609 (2016). https://doi.org/10.1103/PhysRevC.94.014609
34. Z.Q. Feng, Nuclear in-medium effects and collective flows in heavy-ion collisions at intermediate energies. Phys. Rev. C **85**, 014604 (2012). https://doi.org/10.1103/PhysRevC.85.014604
35. Y.F. Guo, P.H. Chen, F. Niu et al., Isospin effect in peripheral heavy-ion collisions at Fermi energies. Chin. Phys. C **42**, 124106 (2018). https://doi.org/10.1088/1674-1137/42/12/124106
36. Z.Q. Feng, Nuclear in-medium and isospin effects on subthreshold kaon production in heavy-ion collisions. Phys. Rev. C **87**, 064605 (2013). https://doi.org/10.1103/PhysRevC.87.064605
37. J. Zenihiro, H. Sakaguchi, S. Terashima *et al*., Direct determination of the neutron skin thicknesses in ^{40,48}Ca from proton elastic scattering at $E_p = 295$ MeV. arXiv:1810.11796 (2018)
38. W.D. Myers, K.H. Schmidt, An update on droplet-model charge distributions. Nucl. Phys. A **410**, 61 (1983). https://doi.org/10.1016/0375-9474(83)90401-3
39. C.W. Ma, Y. Fu, D.Q. Fang et al., A possible experimental observable for the determination of neutron skin thickness. Chin. Phys. B **17**, 1216 (2008). https://doi.org/10.1088/1674-1056/17/4/011
40. R.J. Charity, M.A. McManhan, G.J. Wozniak et al., Systematics of complex fragment emission in niobium-induced reactions. Nucl. Phys. A **483**, 371 (1988). https://doi.org/10.1016/0375-9474(88)90542-8